

# Could the neutrino emission of TXS 0506+056 come from the accretion flow of the supermassive black hole?

QI-RUI YANG,<sup>1,2</sup> RUO-YU LIU,<sup>1,2,3</sup> AND XIANG-YU WANG<sup>1,2</sup>

<sup>1</sup>*School of Astronomy and Space Science, Nanjing University, Nanjing 210023, China; xywang@nju.edu.cn*

<sup>2</sup>*Key laboratory of Modern Astronomy and Astrophysics (Nanjing University), Ministry of Education, Nanjing 210023, China*

<sup>3</sup>*Tianfu Cosmic Ray Research Center, Chengdu 610000, Sichuan, China*

## ABSTRACT

High-energy neutrinos from the blazar TXS 0506+056 are usually thought to arise from the relativistic jet pointing to us. However, the composition of jets of active galactic nuclei (AGNs), whether they are baryon dominated or Poynting flux dominated, is largely unknown. In the latter case, no comic rays and neutrinos would be expected from the AGN jets. In this work, we study whether the neutrino emission from TXS 0506+056 could be powered by the accretion flow of the supermassive black hole. Protons could be accelerated by magnetic reconnection or turbulence in the inner accretion flow. To explain the neutrino flare of TXS 0506+056 in the year of 2014-2015, a super-Eddington accretion is needed. During the steady state, a sub-Eddington accretion flow could power a steady neutrino emission that may explain the long-term neutrino flux from TXS 0506+056. We consider the neutrino production in both magnetically arrested accretion (MAD) flow and the standard and normal evolution (SANE) regime of accretion. In the MAD scenario, due to a high magnetic field, a large dissipation radius is required to avoid the cooling of protons and secondary pions.

## 1. INTRODUCTION

Active Galactic Nuclei (AGN) are prime candidate sources of the high-energy astrophysical neutrinos. In 2017, IceCube detected a high-energy neutrino event in the direction coincident with the blazar TXS 0506+056, which was found to be flaring at the gamma-ray band (IceCube Collaboration et al. 2018a). A follow-up analysis of archival IceCube neutrino data revealed an earlier outburst of neutrinos from the same source in 2014/2015 without an accompanying flare of gamma rays (IceCube Collaboration et al. 2018b). Later, an independent search for point-like sources in the northern hemisphere using ten years of IceCube data revealed that TXS 0506+056 is coincident with the second hottest-spot of the neutrino event excess (IceCube Collaboration et al. 2022). Since blazars are AGNs with relativistic jets pointing toward our line of sight, the Doppler effect remarkably boosts the flux of blazars received by us. Most of the previous studies ascribe the high-energy neutrino emission of TXS 0506+056 to relativistic protons accelerated in the jet, through either photopion production with the radiation of the jet itself and the external radiation of the surrounding environment (e.g. Murase et al. 2018; Keivani et al. 2018; Gao et al. 2019; Cerruti et al. 2019; Rodrigues et al. 2019; Xue et al. 2019; Zhang et al. 2020; Xue et al. 2021), or proton-proton collisions with matter of the jet

and cloud/star entering the jet (e.g. Sahakyan 2018; Liu et al. 2019; Banik et al. 2020; Wang et al. 2022). However, the composition of jets of AGNs, whether they are baryon dominated or Poynting flux dominated, is largely unknown. The composition of jets is tightly related to their formation mechanisms. As discussed by Celotti & Blandford (2001), electromagnetically dominated outflows, such as those generated by the extraction of the spin energy of the black hole, are pair-dominated jets with a low baryonic pollution. In this case, no comic rays and neutrinos would be expected from the AGN jets.

IceCube Collaboration et al. (2022) reported an excess of neutrino events associated with NGC 1068, a nearby type-2 Seyfert galaxy, with a significance of  $4.2\sigma$ . Seyfert galaxies are radio-quiet AGNs with much weaker jets compared to blazars. In NGC 1068, a supermassive black hole (SMBH) at the center is highly obscured by thick gas and dust (Gómez Rosas et al. 2022). X-ray studies have suggested that NGC 1068 is among the brightest AGNs in intrinsic X-rays (Bauer et al. 2015), which is generated through Comptonization of accretion-disk photons in hot plasma above the accretion disk, namely the coronae. Given the dense matter and the intense radiation in the environment, efficient neutrino production is expected if cosmic rays are accelerated at the proximity of the SMBH (Murase

et al. 2020; Inoue et al. 2020). Interestingly, the reported neutrino flux is higher than the GeV gamma-ray flux, implying that gamma-rays above 100 MeV are strongly attenuated by dense X-ray photons while neutrinos can escape.

A correlation between unabsorbed hard X-rays and neutrinos in radio-loud and radio-quiet AGN is suggested by Kun et al. (2024), raising the possibility of a common neutrino production mechanism involved in both types of AGNs. Since neutrino emission from radio-quiet Seyfert galaxies is unlikely related to their weak jets, a natural question arises as to whether neutrinos from blazars can be produced somewhere besides their powerful jets, such as from the proximity of the SMBH.

Hadronic interactions responsible for the neutrino production also generate gamma rays with comparable flux and energy spectra to that of neutrinos. If such interactions take place near the SMBH, where intense infrared-optical photons from the accretion disk and X-rays from the hot corona are present, pair production and subsequent electromagnetic cascade will reprocess the gamma rays into keV-MeV photons. The apparent underproduction of gamma-rays compared to neutrinos in Seyfert galaxies is naturally explained in such environments. A hint of strong gamma-absorption in neutrino sources is also observed in the diffuse neutrino flux (Murase et al. 2020), pointing to the so-called "hidden" neutrino sources.

Motivated by the above reasonings, in this paper, we investigate the possibility that the neutrino outburst of TXS 0506+056 and the steady neutrino emission are produced by the core region of the AGN. Indeed, there have been suggestions that particles may be accelerated in the accretion disk via magnetic reconnection and turbulence (e.g. Yuan et al. 2003; de Gouveia Dal Pino et al. 2010; Hoshino 2013; Kunz et al. 2016; Ripperda et al. 2022; Kheirandish et al. 2021). If the SMBH has a fast-rotating magnetosphere, the centrifugal force may also serve as an efficient particle accelerator (Gangadhara & Lesch 1997; Rieger & Aharonian 2008).

The rest part of the paper is organized as follows. We introduce our model in Section 2 and show the results in Section 3. The discussions are given in Section 4. Finally we summarize the results in Section 5.

## 2. NEUTRINOS FROM THE AGN DISK IN TXS 0506+056 ?

The blazar TXS 0506+056 is the first individual neutrino source identified at  $> 3\sigma$  significance excess and  $13 \pm 5$  high-energy neutrino events was discovered in the period between September 2014 and March 2015. (Ice-

Cube Collaboration et al. 2018b). For this flare period, the neutrino integrated luminosity (per flavor) between 32 TeV and 4 PeV is estimated to be  $L_{\nu_\mu} \sim 10^{47} \text{ erg s}^{-1}$ . The time-integrated analysis of the ten years of Ice-Cube data revealed that TXS 0506+056 is coincident with the second hottest-spot of the neutrino event excess (IceCube Collaboration et al. 2022). A mean flux of  $\sim 10^{-13} \text{ TeV cm}^{-2} \text{ s}^{-1}$  is obtained (IceCube Collaboration et al. 2022), corresponding to a neutrino luminosity of  $L_{\nu_\mu} \sim 5 \times 10^{44} \text{ erg s}^{-1}$ .

The Eddington luminosity of the accretion disk in TXS 0506+056 is estimated to be

$$L_{\text{Edd}} = 4 \times 10^{46} \text{ erg s}^{-1} \left( \frac{M_{\text{BH}}}{3 \times 10^8 M_\odot} \right), \quad (1)$$

where  $M_{\text{BH}}$  is the mass of the supermassive black hole. The Eddington accretion rate is defined as  $\dot{M}_{\text{Edd}} = L_{\text{Edd}}/(\eta_a c^2)$ , where  $\eta_a = 0.1$  (Yuan & Narayan 2014). Assuming an efficiency  $\epsilon_{\text{CR}}$  for accretion power converted into cosmic rays, the cosmic ray luminosity is estimated to be

$$\begin{aligned} L_{\text{CR}} &= \epsilon_{\text{CR}} \dot{M} c^2 \\ &= 4 \times 10^{46} \text{ erg s}^{-1} \left( \frac{\epsilon_{\text{CR}}}{0.1} \right) \left( \frac{\dot{m}}{1} \right) \left( \frac{M_{\text{BH}}}{3 \times 10^8 M_\odot} \right), \end{aligned} \quad (2)$$

where  $\dot{m} = \dot{M}/\dot{M}_{\text{Edd}}$  is the dimensionless accretion rate and we use  $\epsilon_{\text{CR}} = 0.1$  as a fiducial value. Then the neutrino luminosity (per flavor) produced by cosmic rays via  $pp$  or  $p\gamma$  interaction is given by

$$\begin{aligned} L_{\nu_\mu} &= \frac{1}{8} f_{pp,p\gamma} L_{\text{CR}} \\ &\sim 5 \times 10^{45} \text{ erg s}^{-1} f_{pp,p\gamma} \left( \frac{\epsilon_{\text{CR}}}{0.1} \right) \left( \frac{\dot{m}}{1} \right) \left( \frac{M_{\text{BH}}}{3 \times 10^8 M_\odot} \right). \end{aligned} \quad (3)$$

Here  $f_{pp,p\gamma} = t_{\text{loss}}/t_{pp,p\gamma}$  is the efficiency of  $pp$  and  $p\gamma$  processes expressed in the ratio between the proton energy loss timescale ( $t_{\text{loss}}$ ) and the hadronic interaction timescale ( $t_{pp,p\gamma}$ ), which will be calculated in following sections. To explain the observed neutrino luminosity, we require

$$\dot{m} \sim 20 f_{pp,p\gamma}^{-1} \left( \frac{\epsilon_{\text{CR}}}{0.1} \right)^{-1} \left( \frac{M_{\text{BH}}}{3 \times 10^8 M_\odot} \right)^{-1} \left( \frac{L_{\nu_\mu}}{10^{47} \text{ erg s}^{-1}} \right)^{-1}. \quad (4)$$

Therefore, to explain the neutrino flare during 2014-2015, a super-Eddington accretion rate is required. On the other hand, to explain the 10-year quasi-steady-state neutrino emission with a flux 2 orders of magnitude lower, a sub-Eddington accretion may be viable.

### 2.1. The process of proton acceleration and cooling in the accretion flow

High-energy protons may be accelerated by magnetic reconnection, stochastic acceleration via MHD turbulence or electric potential gaps in the black hole magnetosphere. We here do not specify the detailed acceleration mechanism, but phenomenologically parameterize the particle acceleration timescale by

$$t_{\text{acc}} \approx \frac{\eta r_L}{c}, \quad (5)$$

where the different particle acceleration mechanisms may be characterized by distinct parameter  $\eta$ , which could be understood as the particle acceleration efficiency.  $r_L = E/eB$  is the Larmor radius. The maximum energy of non-thermal proton is determined by the balance among particle acceleration, cooling, and escape processes in the accretion flow. The escape term is common for all components. We consider diffusion and advection (infall to the BH) as the escape processes, whose timescales are estimated to be  $t_{\text{diff}} \approx R^2/D_R$  and  $t_{\text{fall}} \approx R/V_R$  respectively, where  $D_R = D_R \approx \eta r_L c/3$  is the diffusion coefficient and  $V_R$  is the radial velocity of the accretion flow. The total escape time is given by  $t_{\text{esc}}^{-1} = t_{\text{diff}}^{-1} + t_{\text{fall}}^{-1}$ .

For the cooling of cosmic ray protons, we consider inelastic collisions ( $pp$ ), photomeson production ( $p\gamma$ ), Bethe-Heitler pair production, and proton synchrotron radiation. The photon field includes the multi-temperature black-body emission from the accretion disk and hard X-ray emission from comptonized corona. The coronal spectrum can be modeled by a power law with an exponential cutoff. The photon index of TXS 0506+056,  $\Gamma_X$ , varies between 1.5 – 1.9 among observations (Acciari et al. 2022). The photon index is correlated with  $\lambda_{\text{Edd}} = L_{\text{bol}}/L_{\text{Edd}} \sim 0.24$  as  $\Gamma_X \approx 0.167 \times \log(\lambda_{\text{Edd}}) + 2.0 = 1.89$  (Padovani et al. 2019; Trakhtenbrot et al. 2019), and the cutoff energy is given by  $\varepsilon_{X,\text{cut}} \sim -74 \log(\lambda_{\text{Edd}}) + 1.5 \times 10 \text{ keV} = 0.19 \text{ MeV}$  (Ricci et al. 2018). We use the average hard X-ray luminosity in 15–55 keV of  $(9.0 \pm 2.4) \times 10^{44} \text{ erg s}^{-1}$  to normalize the quasi-steady state X-ray component (Kun et al. 2024). In the flare state characterized by an accretion rate two orders of magnitude higher, the bolometric luminosity would increase by a factor of 5–6 compared with that in the steady state (Huang et al. 2020).

For the radiation of the disk, we consider a multi-temperature blackbody emission with the maximum temperature near the central supermassive black hole  $T_{\text{disk}} \approx 0.49 (GM_{\text{BH}} \dot{M} / (72\pi \sigma_{\text{SB}} R_S^3))^{1/4} K$  (Pringle 1981). The temperature of the disk can be expressed as  $T(r) \approx (r/R_S)^{-3/4}$ . Here,  $M_{\text{BH}}$  is the SMBH mass,  $R_S = 2GM_{\text{BH}}/c^2$  is the Schwarzschild radius, and  $\sigma_{\text{SB}}$  is the Stefan-Boltzmann constant. We can calculate the

disk luminosity as

$$L_\nu = \frac{8\pi^2 h \nu^3}{c^2} \int_{R_S}^R \frac{r dr}{e^{(h\nu/kT(r))} - 1}. \quad (6)$$

The timescale of photomeson process ( $p\gamma$ ) is  $t_{p\gamma} \approx 1/(n_\gamma \sigma_{p\gamma} \kappa_{p\gamma} c)$ , where  $\sigma_{p\gamma} \approx 5 \times 10^{-28} \text{ cm}^2$  is the cross section for the photomeson process and  $\kappa_{p\gamma} \sim 0.2$  is the inelasticity for  $p\gamma$ . The Bethe-Heitler energy loss rate is  $t_{\text{B-H}} \approx 1/(n_\gamma \hat{\sigma}_{\text{B-H}} c)$ , where  $\hat{\sigma}_{\text{B-H}} \sim 0.8 \times 10^{-30} \text{ cm}^2$  is the effective cross section for the Bethe-Heitler process (Murase et al. 2020). The  $pp$  cooling timescale is  $t_{pp} \approx 1/(n_p \sigma_{pp} \kappa_{pp} c)$ , where  $\sigma_{pp} \approx 4 \times 10^{-26} \text{ cm}^2$  and  $\kappa_{pp} \approx 0.5$  are cross section and inelasticity for  $pp$  process (Kelner et al. 2006). The proton synchrotron timescale is  $t_{p,\text{syn}} = 6\pi m_p c / (\gamma_p \sigma_T B^2)$ . The total cooling rate can be given by  $t_{\text{cool}}^{-1} = t_{p\gamma}^{-1} + t_{pp}^{-1} + t_{\text{syn}}^{-1} + t_{\text{B-H}}^{-1}$ , which is summation of all cooling rate. For high energy protons, the total energy loss rate is  $t_{\text{loss}}^{-1} = t_{\text{esc}}^{-1} + t_{\text{cool}}^{-1}$ .

## 2.2. Proton spectrum

As will be shown later, cooling timescale of high-energy protons is much shorter than the 14–15 outburst duration, so that we may consider a quasi-steady state spectrum for protons. To obtain the non-thermal spectra for protons, we solve the transport equation

$$\frac{d}{dE_p} \left( -\frac{E_p}{t_{\text{cool}}} N_p \right) = \dot{N}_{p,\text{inj}} - \frac{N_p}{t_{\text{esc}}}, \quad (7)$$

where  $N_p = dN/dE_p$ , and  $\dot{N}_{p,\text{inj}}$  is the injection function. We consider the injection as a power-law distribution function with an exponential cutoff

$$\dot{N}_{p,\text{inj}} = \dot{N}_0 E_p^{-s_{\text{inj}}} \exp \left( -\frac{E_p}{E_{p,\text{max}}} \right), \quad (8)$$

which is normalized by

$$\int E_p \dot{N}_{E_p,\text{inj}} dE_p = L_{\text{CR}}. \quad (9)$$

Here we consider the injected proton with spectrum index of  $s_{\text{inj}} = 2$ . The maximum energy  $E_{p,\text{max}}$  will be discussed in the following sections. Then, the steady energy distribution of protons can be obtained approximately by solving the following transport equation,

$$\begin{aligned} \frac{dN_p}{dE_p} &= \frac{t_{\text{cool}}}{E_p} \int_{E_p}^{\infty} dE \dot{N}_{E,\text{inj}} \exp \left( -\int_{E_p}^E \frac{t_{\text{cool}} d\varepsilon_p}{t_{\text{esc}} \varepsilon_p} \right) \\ &\approx \dot{N}_{E_p,\text{inj}} t_{\text{loss}}. \end{aligned} \quad (10)$$

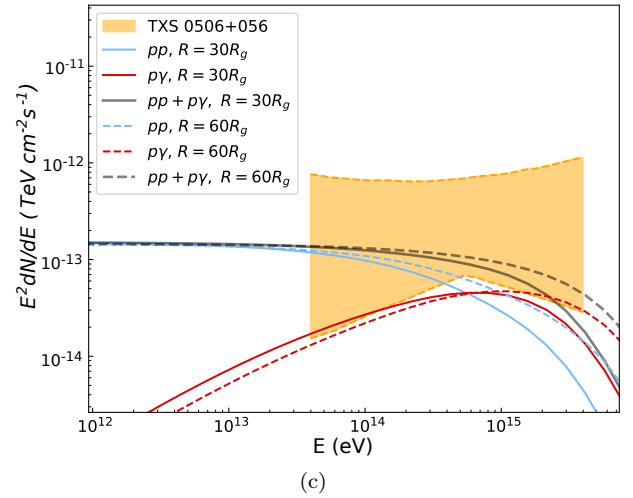
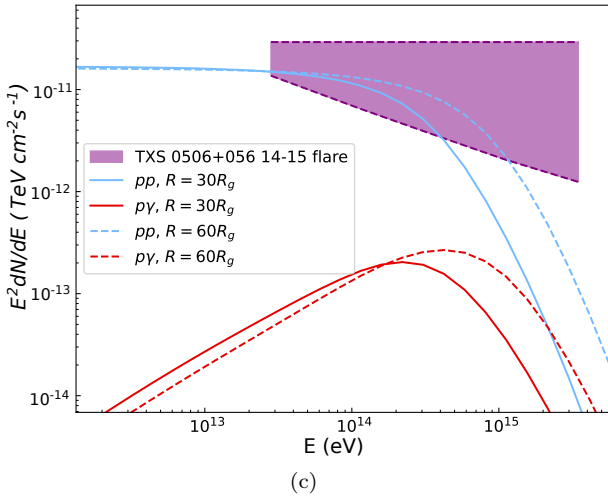
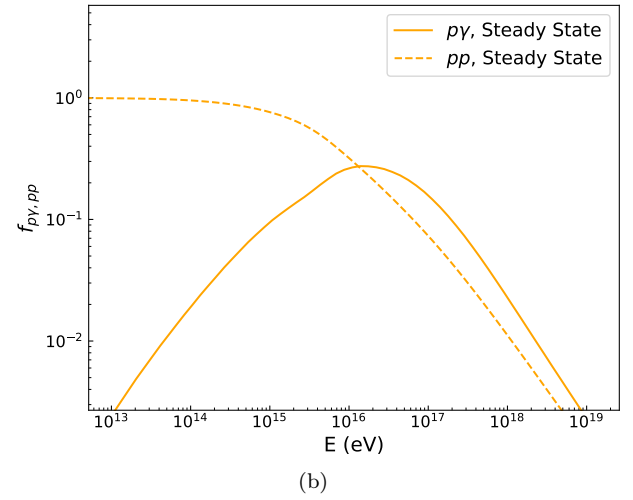
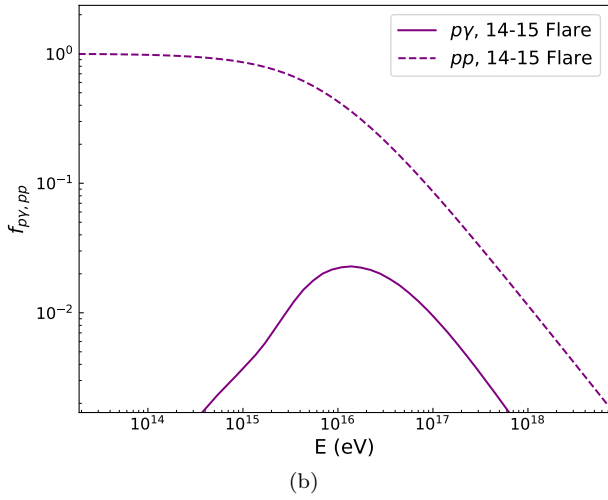
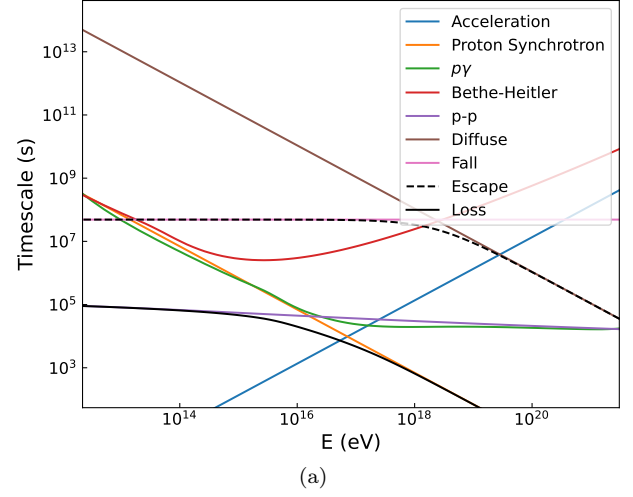
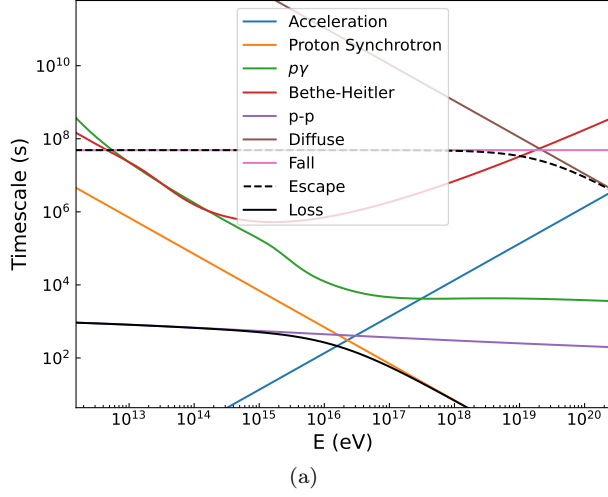


**Figure 1.** The panels, from top to bottom, show the various timescales, the efficiencies of  $pp$  and  $p\gamma$  interactions, and the neutrino spectrum in the MAD scenario. In panel (c), the observed neutrino spectrum of TXS 0506+056 during the 2014-2015 neutrino flare is also shown (IceCube Collaboration et al. 2018b). We adopt the parameter values of  $M_{\text{BH}} = 3 \times 10^8 M_{\odot}$ ,  $\epsilon_{\text{CR}} = 0.1$ ,  $\epsilon = 0.01$ ,  $\eta = 300$  and  $\dot{m} = 10$ . In panel (a) and panel (b), the dissipation radius is set as  $30R_g$ , while in panel (c), two radius with  $R = 30R_g$  and  $R = 60R_g$  are assumed.

**Figure 2.** Same as Fig. 1, but assuming  $\dot{m} = 0.1$  to explain the time-integrated neutrino emission of TXS 0506+056 (IceCube Collaboration et al. 2022).

### 3. NEUTRINO EMISSION FROM THE ACCRETION FLOW IN THE MAD AND SANE SCENARIOS

A magnetically arrested accretion disc (MAD, see Narayan et al. (2003); Bisnovatyi-Kogan & Ruzmaikin (1974); Igumenshchev et al. (2003); Tchekhovskoy et al. (2014)) may be present in TXS 0506+056 since magnetohydrodynamical (MHD) simulations have shown that it can launch powerful jets (e.g. Tchekhovskoy et al. (2011)). In this situation, a large-scale poloidal magnetic field prevents gas from accreting continuously at a magnetospheric radius. Around the magnetospheric radius, the gas flow breaks up into a blob-like stream and moves inward by diffusing via magnetic interchanges through the magnetic field. We also consider the standard and normal evolution (SANE) regime of accretion, where the magnetic field that accumulates around the BH is relatively weak.

#### 3.1. The MAD scenario

MADs dissipate their magnetic energies through plasma processes, such as magnetic reconnection (Ball et al. 2018; Ripperda et al. 2020), and nonthermal particles are efficiently accelerated by reconnection (Hoshino 2012; Sironi & Spitkovsky 2014; Werner et al. 2018) and/or turbulence (Lynn et al. 2014; Kimura et al. 2019). The neutrino production in the super-Eddington accretion phase of the MAD state has been discussed for tidal disruption events (Hayasaki & Yamazaki 2019).

In the MAD scenario, the proton number density in the accretion flow is  $n_{p,\text{MAD}} = \dot{M}/4\pi m_p R H V_{R,\text{MAD}}$ , where  $V_{R,\text{MAD}} = \epsilon V_{\text{ff}}$  is the radial velocity of the accretion flow,  $V_{\text{ff}} = \sqrt{2GM_{\text{BH}}/R}$  is free-fall velocity and  $\epsilon \lesssim 0.01$  (Narayan et al. 2003). Taking disk height  $H = R/2$ , we have

$$n_{p,\text{MAD}} \sim 7.3 \times 10^{12} \text{ cm}^{-3} \left( \frac{\dot{m}}{10} \right) \left( \frac{0.01}{\epsilon} \right) \left( \frac{M_{\text{BH}}}{3 \times 10^8 M_{\odot}} \right)^{1/2} \left( \frac{R}{30 R_g} \right)^{-3/2} \quad (11)$$

Here we consider a dissipation site with a radius  $R \sim 30 - 60 R_g$  for the MAD scenario. For smaller  $R$ , the cooling of protons due to synchrotron emission would be too strong and the neutrino emission will be suppressed (as discussed later).

The magnetic field of MAD can be obtained by equating the magnetic energy density  $B_{\text{MAD}}^2/(8\pi)$  with the gravitational force per unit area of the radially accreting mass  $GM_{\text{BH}}m_p n_{p,\text{MAD}}H/R^2$  (Hayasaki & Yamazaki

2019), which is given by

$$B_{\text{MAD}} = \sqrt{\frac{2GM\dot{M}}{\epsilon V_{\text{ff}} R^3}} \sim 6 \times 10^4 \text{ G} \left( \frac{\dot{m}}{10} \right)^{1/2} \left( \frac{\epsilon}{0.01} \right)^{-1/2} \left( \frac{M_{\text{BH}}}{3 \times 10^8 M_{\odot}} \right)^{3/4} \left( \frac{R}{30 R_g} \right)^{-5/4}. \quad (12)$$

Then the acceleration timescale is given by

$$t_{\text{acc,MAD}} \approx \frac{\eta r_{\text{L}}}{c} \simeq 55 \text{ s} \left( \frac{\dot{m}}{10} \right)^{-1/2} \left( \frac{\epsilon}{0.01} \right)^{1/2} \left( \frac{E_p}{100 \text{ PeV}} \right) \left( \frac{\eta}{300} \right) \left( \frac{M_{\text{BH}}}{3 \times 10^8 M_{\odot}} \right)^{-3/4} \left( \frac{R}{30 R_g} \right)^{5/4}. \quad (13)$$

The timescale of diffusion is  $t_{\text{diff}} \approx R^2/D_{\text{R}} \sim 6.4 \times 10^9 (R/30 R_g)^2 (E_p/2 \text{ PeV})^{-1} \text{ s}$  and the timescale of advection is  $t_{\text{fall}} \approx R/V_{\text{R}} \simeq 1.7 \times 10^7 (R/30 R_g)^{3/2} (\epsilon/0.01)^{-1} (M_{\text{BH}}/3 \times 10^8 M_{\odot})^{-1/2} \text{ s}$  respectively. The  $pp$  cooling timescale is

$$t_{pp,\text{MAD}} \approx 1/n_p \sigma_{pp} \kappa_{pp} c \sim 230 \text{ s} \left( \frac{\dot{m}}{10} \right)^{-1} \left( \frac{M}{3 \times 10^8 M_{\odot}} \right)^{1/2} \left( \frac{R}{30 R_g} \right)^{-3/2}, \quad (14)$$

and the proton synchrotron timescale is

$$t_{p,\text{syn,MAD}} = \frac{6\pi m_p c}{\gamma_p \sigma_T B^2} \left( \frac{m_p}{m_e} \right)^2 \approx 12 \text{ s} \left( \frac{\dot{m}}{10} \right)^{-1} \left( \frac{\epsilon}{0.01} \right) \left( \frac{E_p}{100 \text{ PeV}} \right)^{-1} \left( \frac{M_{\text{BH}}}{3 \times 10^8 M_{\odot}} \right)^{-3/2} \left( \frac{R}{30 R_g} \right)^{5/2}. \quad (15)$$

In the  $p\gamma$  process, the energy of high-energy protons and the energy of target photons is related by  $E_p \epsilon_{\gamma} \sim 0.15 \text{ GeV}^2$ . Therefore, the energy of target photons is  $\epsilon_{\gamma} \sim 1.5 \text{ eV}$  for protons with  $E_p \sim 100 \text{ PeV}$ . The number density of target photons in accretion disk is  $n_{\gamma} = L_{\text{disk}}/4\pi R^2 c \epsilon_0 \approx 3 \times 10^{13} \text{ cm}^{-3} (L_{\text{disk}}/4.7 \times 10^{43} \text{ erg s}^{-1}) (\epsilon_{\gamma}/1.5 \text{ eV})^{-1} (R/30 R_g)^{-2}$ , where  $L_{\text{disk}}$  is the luminosity of the inner disk at 1.5 eV, which is obtained by Eq.(6)

Therefore, the timescale of photomeson process ( $p\gamma$ ) can be estimated as

$$t_{p\gamma,\text{MAD}} \approx 1/n_{\gamma} \sigma_{p\gamma} \kappa_{p\gamma} c \simeq 10^4 \text{ s} \left( \frac{n_{\gamma}}{3 \times 10^{13} \text{ cm}^{-3}} \right)^{-1}, \quad (16)$$

and the Bethe-Heitler timescale  $t_{\text{B-H}}$  is

$$t_{\text{B-H,MAD}} \approx 1/n_{\gamma} \hat{\sigma}_{\text{BH}} c \simeq 1.4 \times 10^6 \text{ s} \left( \frac{n_{\gamma}}{3 \times 10^{13} \text{ cm}^{-3}} \right)^{-1}. \quad (17)$$

Comparing the estimated timescales in Eq.(16), Eq.(17), Eq.(14) and Eq.(15), we find that the proton

synchrotron process dominates the cooling in the MAD scenario for typical parameter values. By equating the acceleration timescale in Eq.(13) and the proton synchrotron timescale in Eq.(15), we can derive the maximum proton energy,

$$E_{p,\text{max,MAD}} \approx 50 \text{ PeV} \left( \frac{\dot{m}}{10} \right)^{-1/4} \left( \frac{R}{30R_g} \right)^{-5/8} \left( \frac{M_{\text{BH}}}{3 \times 10^8 M_\odot} \right)^{3/8} \left( \frac{\eta}{300} \right)^{-1/2}. \quad (18)$$

We show the various timescales in the panel (a) of Fig. 1 for  $R = 30R_g$  and  $R = 60R_g$  with super-Eddington accretion  $\dot{m} = 10$ . We used strict expressions of  $p\gamma$  and Bethe-Heitler process

$$t_{p\gamma, \text{B-H}}^{-1} = \frac{c}{2\gamma_p^2} \int_{\epsilon_{\text{th}}}^{\infty} \sigma(\bar{\epsilon}) \kappa(\bar{\epsilon}) \bar{\epsilon} d\bar{\epsilon} \int_{\bar{\epsilon}/2\gamma_p}^{\infty} \epsilon^{-2} \frac{dn}{d\epsilon} d\epsilon, \quad (19)$$

in calculating the relevant timescales,  $\gamma_p$  is Lorentz factors of protons,  $\bar{\epsilon}$  is the photon energy in the proton rest frame,  $dn/d\epsilon$  is the number density of target photons,  $\epsilon_{\text{th}}$  is the threshold energy of  $p\gamma$  or Bethe-Heitler process,  $\sigma$  is cross-section and  $\kappa$  is inelasticity for  $p\gamma$  or Bethe-Heitler process. Note that the acceleration timescale required for protons to reach the maximum energy of 50 PeV is on the order of  $10^3 - 10^4$ s, which is much shorter than the duration of the 2014-2015 flare. Thus, the flare duration does not affect the maximum energy of accelerated protons.

For protons energy below 100 TeV,  $pp$  collision dominates the cooling process and  $p\gamma$  is partly suppressed by the proton synchrotron emission in the energy range of 320 TeV to 32 PeV. From the above timescales, we can derive  $pp$  and  $p\gamma$  interaction efficiencies, which are shown in the panel (b) of Fig. 1. The efficiencies of  $pp$  and  $p\gamma$  process in the relevant proton energy range are roughly  $f_{pp} \sim 0.9$  and  $f_{p\gamma} \sim 0.01$  for typical parameter values, respectively. Hence, during the 2014-2015 neutrino flare period, the neutrino production is predominantly produced by  $pp$  collisions.

In panel (c) of Fig. 1, we show the neutrino spectrum in comparison with the observations by IceCube during the 2014-2015 neutrino flare period of TXS 0506+056. The solid line represents the neutrino spectrum for  $R = 60R_g$ , whereas the dashed line represents the neutrino spectrum for  $R = 30R_g$ . A smaller radius of the dissipation site leads to a larger magnetic field, thereby increasing the cooling of pions as well as protons and leading to a lower cutoff energy in the neutrino spectrum. Note that here it is the pion cooling that determines the cutoff energy in the neutrino spectrum, since the pion cooling is stronger than the proton cooling at high energies for typical parameter values.

We also consider the steady-state neutrino emission of TXS 0506+056 in the MAD scenario, where a lower accretion rate is applicable. We consider a sub-Eddington accretion rate with  $\dot{m} \sim 0.1$  for TXS 0506+056. The corresponding timescales, the  $pp$  and  $p\gamma$  efficiency, and the neutrino spectrum are shown in Fig. 2. We find that  $pp$  process still dominates the  $p\gamma$  process for typical parameter values and this scenario can explain the 10-year time-integrated neutrino emission observed by IceCube (IceCube Collaboration et al. 2022).

### 3.2. The SANE scenario

In the SANE scenario, a lower magnetic field is expected in the accretion flow. We set the plasma  $\beta$  as  $\beta = 10$ . The proton number density in the accretion flow is

$$n_{p,\text{SANE}} \sim 2.7 \times 10^{11} \text{ cm}^{-3} \left( \frac{\dot{m}}{10} \right) \left( \frac{0.3}{\alpha} \right) \left( \frac{M_{\text{BH}}}{3 \times 10^8 M_\odot} \right)^{1/2} \left( \frac{R}{30R_g} \right)^{-3/2}, \quad (20)$$

where the radial velocity is  $V_{\text{R,SANE}} \approx \alpha V_k/2$  in the SANE scenario,  $V_k = \sqrt{GM/R}$  is Keplerian velocity and  $\alpha \sim 0.3$  is the viscous parameter. Then the magnetic field is given by

$$B_{\text{SANE}} = \sqrt{\frac{8\pi n_{p,\text{SANE}} m_p C_s^2}{\beta}} \sim 2.5 \times 10^3 \text{ G} \left( \frac{\dot{m}}{10} \right)^{1/2} \left( \frac{\beta}{10} \right)^{-1/2} \left( \frac{M_{\text{BH}}}{3 \times 10^8 M_\odot} \right)^{3/4} \left( \frac{R}{30R_g} \right)^{-5/4} \left( \frac{\alpha}{0.3} \right)^{-1/2}, \quad (21)$$

where  $C_s \approx V_k/2$  is sound speed. The particle acceleration timescale is given by

$$t_{\text{acc,SANE}} \simeq 1.3 \times 10^3 \text{ s} \left( \frac{\dot{m}}{10} \right)^{-1/2} \left( \frac{\beta}{10} \right)^{1/2} \left( \frac{E_p}{100 \text{ PeV}} \right) \left( \frac{\eta}{300} \right) \left( \frac{M_{\text{BH}}}{3 \times 10^8 M_\odot} \right)^{-3/4} \left( \frac{R}{30R_g} \right)^{5/4} \left( \frac{\alpha}{0.3} \right)^{1/2}. \quad (22)$$

The timescale of diffusion is  $t_{\text{diff}} \approx R^2/D_{\text{R}} \sim 2.6 \times 10^8 \text{ s} (R/30R_g)^2 (E_p/100 \text{ PeV})^{-1}$  and  $t_{\text{fall}} \approx R/V_{\text{R}} \simeq 1.6 \times 10^6 \text{ s} (R/30R_g)^{3/2} (\alpha/0.3)^{-1} (M_{\text{BH}}/3 \times 10^8 M_\odot)^{-1/2}$  respectively. The cooling timescales of  $pp$  collision and proton synchrotron emission are, respectively,

$$t_{pp,\text{SANE}} \sim 6 \times 10^3 \text{ s} \left( \frac{\dot{m}}{10} \right)^{-1} \left( \frac{\alpha}{0.3} \right) \left( \frac{M_{\text{BH}}}{3 \times 10^8 M_\odot} \right)^{-1/2} \left( \frac{R}{30R_g} \right)^{3/2} \quad (23)$$

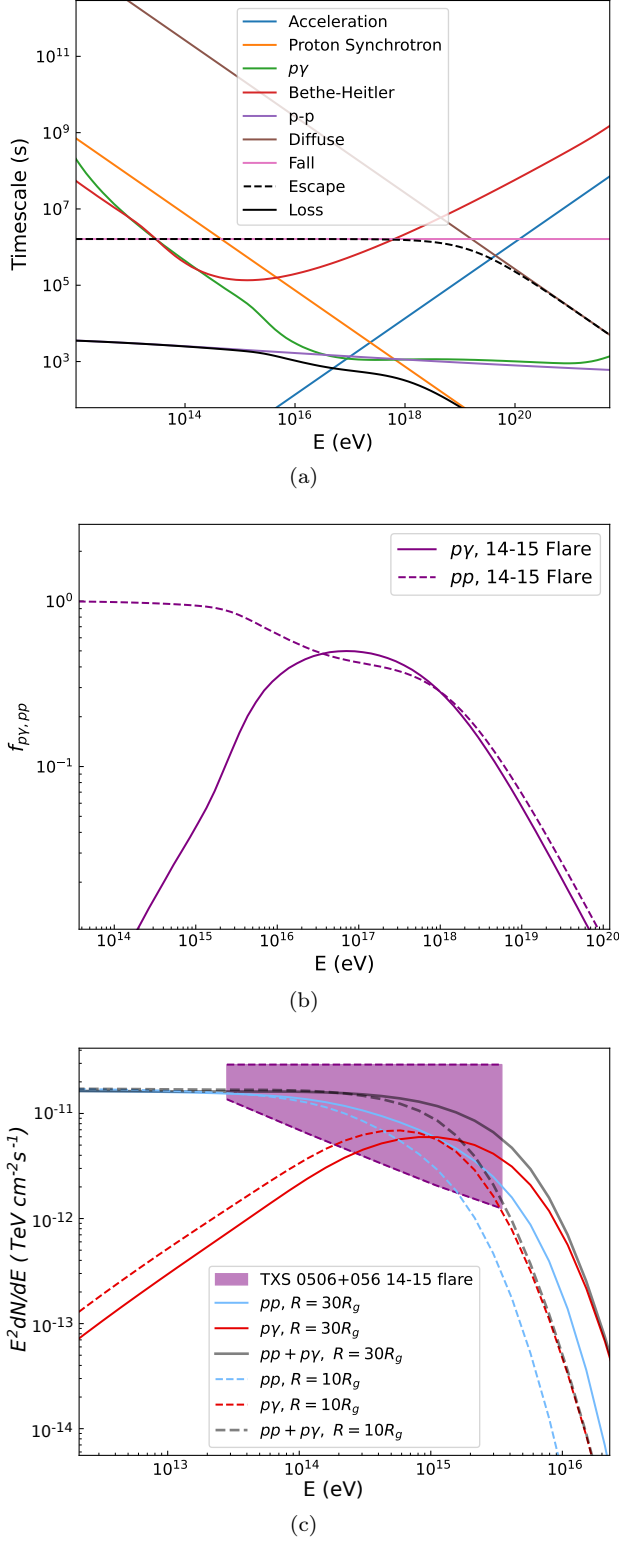


**Figure 3.** The panels, from top to bottom, show the various timescales, the efficiencies of  $pp$  and  $p\gamma$  interactions, and the neutrino spectrum in the SANE scenario. We adopt the parameters  $M_{\text{BH}} = 3 \times 10^8 M_{\odot}$ ,  $\epsilon_{\text{CR}} = 0.1$ ,  $\alpha = 0.3$ ,  $\beta = 10$ ,  $\eta = 300$ ,  $\beta = 10$  and  $\dot{m} = 10$ . For panel (a) and panel (b), the dissipation radius is set as  $30R_g$ , while in panel (c), two radius with  $R = 10R_g$  and  $R = 30R_g$  are assumed. In panel (c), the observed neutrino spectrum of TXS 0506+056 during the 2014-2015 neutrino flare is also shown.

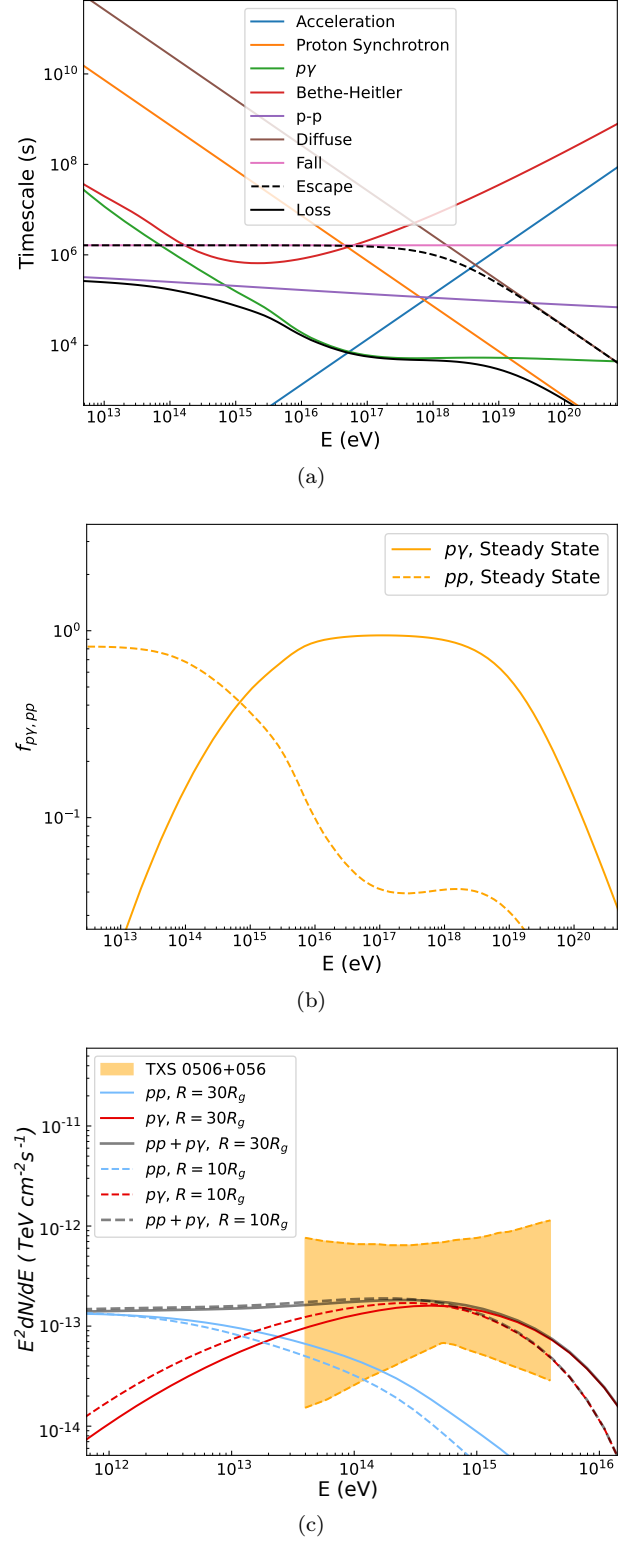


**Figure 4.** Same as Fig. 3, but assuming  $\dot{m} = 0.1$  to explain the time-integrated neutrino emission of TXS 0506+056 (Ice-Cube Collaboration et al. 2022).

and

$$t_{p,\text{syn,SANE}} \sim 7 \times 10^3 \text{ s} \left( \frac{\dot{m}}{10} \right)^{-1} \left( \frac{\beta}{10} \right) \left( \frac{E_p}{100 \text{ PeV}} \right)^{-1} \left( \frac{M_{\text{BH}}}{3 \times 10^8 M_\odot} \right)^{-3/2} \left( \frac{R}{30 R_g} \right)^{5/2} \left( \frac{\alpha}{0.3} \right). \quad (24)$$

For the photon field in the SANE scenario, the number density of target photons is estimated to be  $n_\gamma = L_{\text{disk}}/4\pi R^2 c \varepsilon_0 \approx 3 \times 10^{13} \text{ cm}^{-3} (L_{\text{disk}}/4.7 \times 10^{43} \text{ erg s}^{-1})(\varepsilon_0/1.5 \text{ eV})^{-1}(R/30 R_g)^{-2}$ . Then the timescale of photomeson process ( $p\gamma$ ) can be estimated as

$$t_{p\gamma,\text{SANE}} \simeq 10^4 \text{ s} \left( \frac{n_\gamma}{3 \times 10^{13} \text{ cm}^{-3}} \right)^{-1}, \quad (25)$$

and the timescale of Bethe-Heitler is

$$t_{\text{B-H,SANE}} \simeq 1.4 \times 10^6 \text{ s} \left( \frac{n_\gamma}{3 \times 10^{13} \text{ cm}^{-3}} \right)^{-1}. \quad (26)$$

From the timescales above, we find that in the SANE scenario, depending on the parameter values, the  $pp$ ,  $p\gamma$  and the proton synchrotron emission processes all could become the dominant cooling mechanism for the highest energy protons. If the  $pp$  process becomes the dominant mechanism for the proton cooling, by equating the acceleration timescale with the  $pp$  cooling timescale, we obtain the maximum proton energy,

$$E_{p,\text{max,SANE}} \approx 400 \text{ PeV} \left( \frac{\dot{m}}{10} \right)^{-1/2} \left( \frac{M_{\text{BH}}}{3 \times 10^8 M_\odot} \right)^{1/4} \left( \frac{R}{30 R_g} \right)^{1/4} \left( \frac{\beta}{10} \right)^{-1/2} \left( \frac{\alpha}{0.3} \right)^{1/2} \left( \frac{\eta}{300} \right)^{-1}. \quad (27)$$

Similarly, if the  $p\gamma$  process becomes the predominant mechanism for the proton cooling, the maximum energy is

$$E_{p,\text{max,SANE}} \approx 800 \text{ PeV} \left( \frac{\dot{m}}{10} \right)^{1/2} \left( \frac{M_{\text{BH}}}{3 \times 10^8 M_\odot} \right)^{3/4} \left( \frac{R}{30 R_g} \right)^{-5/4} \left( \frac{\beta}{10} \right)^{-1/2} \left( \frac{\alpha}{0.3} \right)^{-1/2} \left( \frac{n_\gamma}{3 \times 10^{13} \text{ cm}^{-3}} \right)^{-1} \left( \frac{\eta}{300} \right)^{-1}, \quad (28)$$

and if the proton synchrotron emission becomes the predominant mechanism for the proton cooling, the maxi-

mum energy is

$$E_{p,\text{max,SANE}} = 250 \text{ PeV} \left( \frac{\dot{m}}{10} \right)^{-1/4} \left( \frac{\beta}{10} \right)^{1/4} \left( \frac{M_{\text{BH}}}{3 \times 10^8 M_\odot} \right)^{-3/8} \left( \frac{R}{30 R_g} \right)^{5/8} \left( \frac{\alpha}{0.3} \right)^{1/4} \left( \frac{\eta}{300} \right)^{-1/2}. \quad (29)$$

The panel (a) of Fig. 3 shows various timescales in the SANE scenario for a dissipation radius of  $R = 30 R_g$ . For low-energy protons, the cooling is dominantly by  $pp$  interactions, whereas for the high-energy protons the cooling of both  $p\gamma$  interaction and proton synchrotron emission are important. The efficiency for  $pp$  and  $p\gamma$  are shown in panel (b) of Fig. 3, which gives  $f_{pp} \sim 1$  and  $f_{p\gamma} \sim 0.6$  in the neutrino energy range where the respective cooling process is dominated. In panel (c) of Fig. 3, we show the neutrino spectrum in comparison with the observation data during the 2014-2015 neutrino flare period of TXS 0506+056. Owing to a reduced magnetic field in the SANE scenario, the size of the dissipation region could be considerably smaller without suffering from a strong cooling for protons. Therefore we consider two dissipation radii with  $R = 10 R_g$  and  $R = 30 R_g$ , respectively. We find that  $pp$  and  $p\gamma$  processes contribute significantly to the neutrino flux at lower and higher energies, respectively.

Same as the MAD scenario, we also consider the steady-state neutrino emission of TXS 0506+056 assuming a low accretion rate  $\dot{m} \sim 0.1$ . The corresponding timescales, the  $pp$  and  $p\gamma$  efficiencies, and the neutrino spectrum are shown in Fig. 4. Due to a lower density in the accretion flow, the  $pp$  efficiency becomes lower. As a result, the  $p\gamma$  process becomes dominant in the neutrino production in the observed energy range by IceCube.

#### 4. DISCUSSIONS

We have assumed  $\eta = 300$  in the above calculations. However, the value of  $\eta$  depends on the specific acceleration mechanism. If the acceleration efficiency is lower,  $\eta$  could be significantly larger. We study its influence on the neutrino spectrum in the MAD and SANE scenarios by replacing  $\eta = 300$  with  $\eta = 3000$  and  $\eta = 30000$  in the calculation. Fig. 5 and Fig. 6 show the neutrino spectrum in the MAD and SANE scenarios with various acceleration efficiency  $\eta$ , respectively. In the super-Eddington accretion MAD case (the left panel of Fig. 5), we find that the neutrino spectrum remains almost unchanged between  $\eta = 300$  and  $\eta = 3000$ . This is because the pion cooling is still dominated over the proton synchrotron cooling, although  $E_{p,\text{max}}$  decreases by a factor of 3. However, for  $\eta = 30000$ , the neutrino

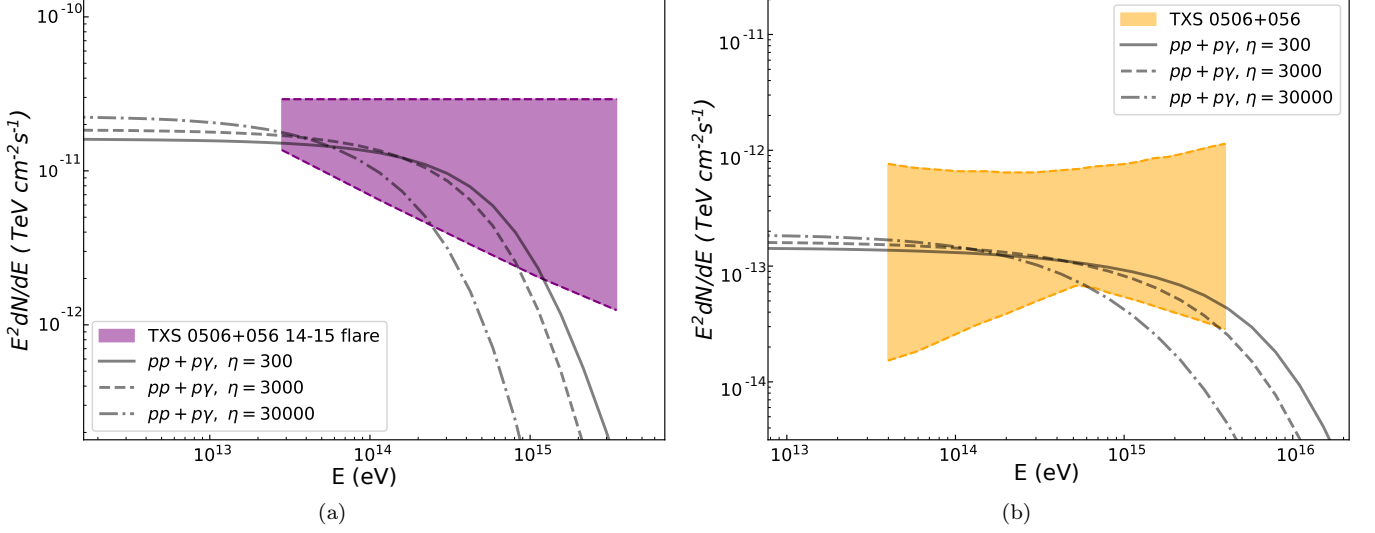


**Figure 5.** The neutrino spectrum with different acceleration efficiency  $\eta$  in the MAD scenario. The parameter values used are:  $R = 60R_g$ ,  $M_{\text{BH}} = 3 \times 10^8 M_\odot$ ,  $\epsilon_{\text{CR}} = 0.1$ , and  $\epsilon = 0.01$ . The solid line, the dashed line and the dot-dashed line represent  $\eta = 300$ ,  $\eta = 3000$  and  $\eta = 30000$ , respectively. The left panel shows the super-Eddington regime ( $\dot{m} = 10$ ) for the 2014-2015 neutrino flare of TXS 0506+056, whereas the right panel shows the sub-Eddington accretion regime ( $\dot{m} = 0.1$ ) for the steady-state emission.

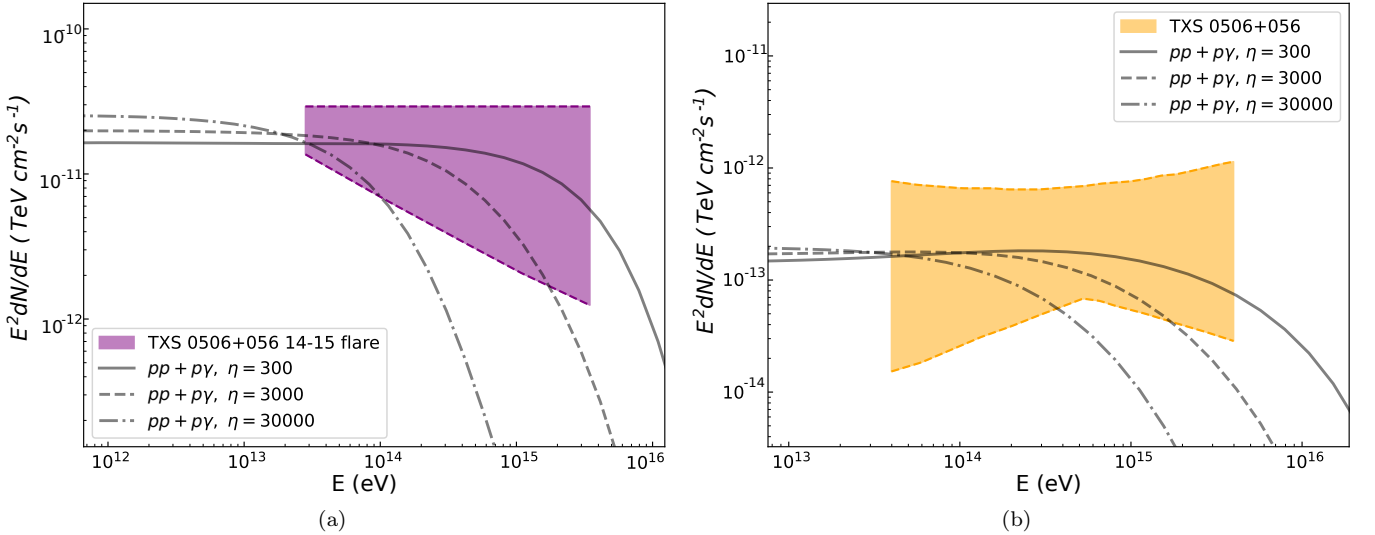


**Figure 6.** Same as Fig. 5, but for the SANE scenario. The parameter values used are:  $R = 30R_g$ ,  $M_{\text{BH}} = 3 \times 10^8 M_\odot$ ,  $\epsilon_{\text{CR}} = 0.1$ ,  $\alpha = 0.3$ , and  $\beta = 10$ .

spectrum softens significantly following the decrease of  $E_{p,\text{max}}$ . In the sub-Eddington accretion MAD case (the right panel of Fig. 5), the situation is quite similar, although the cutoff energy of the neutrino spectrum is higher due to a larger  $E_{p,\text{max}}$  for smaller accretion rate (see Eq.(18)). In the SANE scenario, as  $\eta$  increases and  $E_{p,\text{max}}$  decreases, the cutoff energy of the neutrino spectrum decreases almost in a linear relation with  $\eta$  in both super-Eddington accretion and sub-Eddington accretion regimes. For  $\eta = 30000$ , the neutrino spectrum is too

soft to explain the data. Therefore, to explain the observed neutrino spectrum of TXS 0506+056, we need an acceleration efficiency  $\eta < 30000$  in both MAD and SANE scenarios.

GeV-TeV gamma-rays are observed from TXS 0506+056. Based on the  $\gamma\gamma$  optical depth calculations by (Murase et al. 2020),  $\gamma\gamma$  absorption in the compact corona and accretion disk can effectively suppress GeV-TeV gamma-ray emission from hadronic processes (i.e. the so-called hidden gamma-ray source). The observed

GeV-TeV gamma rays from TXS 0506+056 may then arise from the jets, as usually assumed for GeV-TeV blazars (Madejski & Sikora 2016; Gao et al. 2019; Liu et al. 2023). These emissions are produced through synchrotron self-Compton (SSC) and/or external Compton (EC) processes of relativistic leptons. Being far from the compact corona/disk, these high-energy gamma-rays can avoid absorption and become detectable.

Most previous studies have suggested that the high-energy neutrinos from TXS 0506+056 originate from the relativistic jet in a region with a radius much larger than that of the accretion flow (Gao et al. 2019; Keivani et al. 2018; Cerruti et al. 2019). One way to distinguish between our accretion flow model and the jet model is through the cascade emission induced by the absorbed high-energy gamma-rays accompanying the neutrino production. The compact size of the neutrino production region in the accretion flow model leads to strong absorption of the high-energy gamma-rays and the absorbed energy is transferred to MeV emission through the electromagnetic cascades (Murase et al. 2020). Future mission such as AMEGO-X (Caputo et al. 2022) and eASTROGAM (De Angelis et al. 2017) can detect the MeV emission and test the accretion flow model. In addition, our model predicts that mis-aligned blazars (i.e., radio galaxies), where the jets do not point toward us, can also produce high-energy neutrinos through the accretion flow. Future observations by next-generation neutrino telescopes, such as IceCube-Gen2 (IceCube-Gen2 Collaboration 2023) and HUNT (Huang et al. 2024) can test this.

## 5. SUMMARY

In this work, we study whether the neutrino emission from TXS 0506+056 could come from the accretion flow, instead of the usually discussed relativistic jet. We find that a super-Eddington accretion with  $\dot{M} \sim 10\dot{M}_{\text{Edd}}$  is needed to explain the neutrino outburst during 2014-2015. The accretion flow may also produce the long-

term neutrino emission during the steady state when the accretion drops to sub-Eddington rate. The accretion flow could be a MAD with highly magnetized plasma. Magnetic reconnections and/or plasma turbulence in the MAD may accelerate cosmic ray particles, which produce neutrinos via  $pp$  and  $p\gamma$  processes. Compared with the SANE accretion flow, the MAD has a higher magnetic field, which leads to stronger cooling of cosmic ray protons and secondary pions. As a result, a larger radius for the dissipation in the MAD scenario is needed to avoid this cooling effect. The size of the neutrino production site is still sufficiently compact so that the TeV-PeV gamma-rays accompanied the neutrinos are absorbed by the dense optical to X-ray photons in the AGN core region.

In a super-Eddington accretion flow,  $pp$  interactions play a dominant role in producing neutrinos because of the high density of the accretion flow. This leads to a flat neutrino spectrum with a high-energy cutoff, which is different from the spectrum of neutrino emission produced in the  $p\gamma$  process. This may explain the hard neutrino spectrum in TXS 0506+056 during 2014-2015, in contrast to the soft spectrum of neutrino emission of NGC 1068, which is usually thought to be produced by the  $p\gamma$  process.

## 6. ACKNOWLEDGEMENTS

We would like to thank Haoning He for helpful discussions on the long-term neutrino flux from TXS 0506+056. This work is supported by the National Natural Science Foundation of China (grant Nos. 12333006 and 12121003, 12393852). We are grateful to the High Performance Computing Center (HPCC) of Nanjing University for doing the numerical calculations in this paper on its blade cluster system.

Note added.— While we were finalizing this manuscript, we became aware of the work of Zathul et al. (2024) (arXiv:24.14598), which also propose that the neutrino emission from TXS 0506+056 could originate near its AGN core.

## REFERENCES

- Acciari, V. A., Aniello, T., Ansoldi, S., et al. 2022, ApJ, 927, 197, doi: [10.3847/1538-4357/ac531d](https://doi.org/10.3847/1538-4357/ac531d)
- Ball, D., Özel, F., Psaltis, D., Chan, C.-K., & Sironi, L. 2018, ApJ, 853, 184, doi: [10.3847/1538-4357/aaa42f](https://doi.org/10.3847/1538-4357/aaa42f)
- Banik, P., Bhadra, A., Pandey, M., & Majumdar, D. 2020, PhRvD, 101, 063024, doi: [10.1103/PhysRevD.101.063024](https://doi.org/10.1103/PhysRevD.101.063024)
- Bauer, F. E., Arévalo, P., Walton, D. J., et al. 2015, ApJ, 812, 116, doi: [10.1088/0004-637X/812/2/116](https://doi.org/10.1088/0004-637X/812/2/116)
- Bisnovatyi-Kogan, G. S., & Ruzmaikin, A. A. 1974, Ap&SS, 28, 45, doi: [10.1007/BF00642237](https://doi.org/10.1007/BF00642237)
- Caputo, R., Ajello, M., Kierans, C. A., et al. 2022, Journal of Astronomical Telescopes, Instruments, and Systems, 8, 044003, doi: [10.1117/1.JATIS.8.4.044003](https://doi.org/10.1117/1.JATIS.8.4.044003)
- Celotti, A., & Blandford, R. D. 2001, in Black Holes in Binaries and Galactic Nuclei, ed. L. Kaper, E. P. J. V. D. Heuvel, & P. A. Woudt, 206, doi: [10.1007/10720995\\_43](https://doi.org/10.1007/10720995_43)

- Cerruti, M., Zech, A., Boisson, C., et al. 2019, *MNRAS*, 483, L12, doi: [10.1093/mnrasl/sly210](https://doi.org/10.1093/mnrasl/sly210)
- De Angelis, A., Tatischeff, V., Tavani, M., et al. 2017, *Experimental Astronomy*, 44, 25, doi: [10.1007/s10686-017-9533-6](https://doi.org/10.1007/s10686-017-9533-6)
- de Gouveia Dal Pino, E. M., Piovezan, P. P., & Kadowaki, L. H. S. 2010, *A&A*, 518, A5, doi: [10.1051/0004-6361/200913462](https://doi.org/10.1051/0004-6361/200913462)
- Gómez Rosas, V., Isbell, J. W., Jaffe, W., et al. 2022, *Nature*, 602, 403, doi: [10.1038/s41586-021-04311-7](https://doi.org/10.1038/s41586-021-04311-7)
- Gangadhara, R. T., & Lesch, H. 1997, *A&A*, 323, L45, doi: [10.48550/arXiv.astro-ph/9707182](https://doi.org/10.48550/arXiv.astro-ph/9707182)
- Gao, S., Fedynitch, A., Winter, W., & Pohl, M. 2019, *Nature Astronomy*, 3, 88, doi: [10.1038/s41550-018-0610-1](https://doi.org/10.1038/s41550-018-0610-1)
- Hayasaki, K., & Yamazaki, R. 2019, *ApJ*, 886, 114, doi: [10.3847/1538-4357/ab44ca](https://doi.org/10.3847/1538-4357/ab44ca)
- Hoshino, M. 2012, *PhRvL*, 108, 135003, doi: [10.1103/PhysRevLett.108.135003](https://doi.org/10.1103/PhysRevLett.108.135003)
- . 2013, *ApJ*, 773, 118, doi: [10.1088/0004-637X/773/2/118](https://doi.org/10.1088/0004-637X/773/2/118)
- Huang, J., Luo, B., Du, P., et al. 2020, *ApJ*, 895, 114, doi: [10.3847/1538-4357/ab9019](https://doi.org/10.3847/1538-4357/ab9019)
- Huang, T. Q., Cao, Z., Chen, M., et al. 2024, in 38th International Cosmic Ray Conference, 1080
- IceCube Collaboration, Aartsen, M. G., Ackermann, M., et al. 2018a, *Science*, 361, eaat1378, doi: [10.1126/science.aat1378](https://doi.org/10.1126/science.aat1378)
- . 2018b, *Science*, 361, 147, doi: [10.1126/science.aat2890](https://doi.org/10.1126/science.aat2890)
- IceCube Collaboration, Abbasi, R., Ackermann, M., et al. 2022, *Science*, 378, 538, doi: [10.1126/science.abg3395](https://doi.org/10.1126/science.abg3395)
- IceCube-Gen2 Collaboration. 2023, in APS Meeting Abstracts, Vol. 2023, APS April Meeting Abstracts, D13.008
- Igumenshchev, I. V., Narayan, R., & Abramowicz, M. A. 2003, *ApJ*, 592, 1042, doi: [10.1086/375769](https://doi.org/10.1086/375769)
- Inoue, Y., Khangulyan, D., & Doi, A. 2020, *ApJL*, 891, L33, doi: [10.3847/2041-8213/ab7661](https://doi.org/10.3847/2041-8213/ab7661)
- Keivani, A., Murase, K., Petropoulou, M., et al. 2018, *ApJ*, 864, 84, doi: [10.3847/1538-4357/aad59a](https://doi.org/10.3847/1538-4357/aad59a)
- Kelner, S. R., Aharonian, F. A., & Bugayov, V. V. 2006, *PhRvD*, 74, 034018, doi: [10.1103/PhysRevD.74.034018](https://doi.org/10.1103/PhysRevD.74.034018)
- Kheirandish, A., Murase, K., & Kimura, S. S. 2021, *ApJ*, 922, 45, doi: [10.3847/1538-4357/ac1c77](https://doi.org/10.3847/1538-4357/ac1c77)
- Kimura, S. S., Tomida, K., & Murase, K. 2019, *MNRAS*, 485, 163, doi: [10.1093/mnras/stz329](https://doi.org/10.1093/mnras/stz329)
- Kun, E., Bartos, I., Becker Tjus, J., et al. 2024, arXiv e-prints, arXiv:2404.06867, doi: [10.48550/arXiv.2404.06867](https://doi.org/10.48550/arXiv.2404.06867)
- Kunz, M. W., Stone, J. M., & Quataert, E. 2016, *PhRvL*, 117, 235101, doi: [10.1103/PhysRevLett.117.235101](https://doi.org/10.1103/PhysRevLett.117.235101)
- Liu, R.-Y., Wang, K., Xue, R., et al. 2019, *PhRvD*, 99, 063008, doi: [10.1103/PhysRevD.99.063008](https://doi.org/10.1103/PhysRevD.99.063008)
- Liu, R.-Y., Xue, R., Wang, Z.-R., Tan, H.-B., & Böttcher, M. 2023, *MNRAS*, 526, 5054, doi: [10.1093/mnras/stad2911](https://doi.org/10.1093/mnras/stad2911)
- Lynn, J. W., Quataert, E., Chandran, B. D. G., & Parrish, I. J. 2014, *ApJ*, 791, 71, doi: [10.1088/0004-637X/791/1/71](https://doi.org/10.1088/0004-637X/791/1/71)
- Madejski, G. G., & Sikora, M. 2016, *ARA&A*, 54, 725, doi: [10.1146/annurev-astro-081913-040044](https://doi.org/10.1146/annurev-astro-081913-040044)
- Murase, K., Kimura, S. S., & Mészáros, P. 2020, *PhRvL*, 125, 011101, doi: [10.1103/PhysRevLett.125.011101](https://doi.org/10.1103/PhysRevLett.125.011101)
- Murase, K., Oikonomou, F., & Petropoulou, M. 2018, *The Astrophysical Journal*, 865, 124, doi: [10.3847/1538-4357/aada00](https://doi.org/10.3847/1538-4357/aada00)
- Narayan, R., Igumenshchev, I. V., & Abramowicz, M. A. 2003, *PASJ*, 55, L69, doi: [10.1093/pasj/55.6.L69](https://doi.org/10.1093/pasj/55.6.L69)
- Padovani, P., Oikonomou, F., Petropoulou, M., Giommi, P., & Resconi, E. 2019, *MNRAS*, 484, L104, doi: [10.1093/mnrasl/slz011](https://doi.org/10.1093/mnrasl/slz011)
- Pringle, J. E. 1981, *ARA&A*, 19, 137, doi: [10.1146/annurev.aa.19.090181.001033](https://doi.org/10.1146/annurev.aa.19.090181.001033)
- Ricci, C., Ho, L. C., Fabian, A. C., et al. 2018, *MNRAS*, 480, 1819, doi: [10.1093/mnras/sty1879](https://doi.org/10.1093/mnras/sty1879)
- Rieger, F. M., & Aharonian, F. A. 2008, *A&A*, 479, L5, doi: [10.1051/0004-6361:20078706](https://doi.org/10.1051/0004-6361:20078706)
- Ripperda, B., Bacchini, F., & Philippov, A. A. 2020, *ApJ*, 900, 100, doi: [10.3847/1538-4357/ababab](https://doi.org/10.3847/1538-4357/ababab)
- Ripperda, B., Liska, M., Chatterjee, K., et al. 2022, *ApJL*, 924, L32, doi: [10.3847/2041-8213/ac46a1](https://doi.org/10.3847/2041-8213/ac46a1)
- Rodrigues, X., Gao, S., Fedynitch, A., Palladino, A., & Winter, W. 2019, *ApJL*, 874, L29, doi: [10.3847/2041-8213/ab1267](https://doi.org/10.3847/2041-8213/ab1267)
- Sahakyan, N. 2018, *ApJ*, 866, 109, doi: [10.3847/1538-4357/aadade](https://doi.org/10.3847/1538-4357/aadade)
- Sironi, L., & Spitkovsky, A. 2014, *ApJL*, 783, L21, doi: [10.1088/2041-8205/783/1/L21](https://doi.org/10.1088/2041-8205/783/1/L21)
- Tchekhovskoy, A., Metzger, B. D., Giannios, D., & Kelley, L. Z. 2014, *MNRAS*, 437, 2744, doi: [10.1093/mnras/stt2085](https://doi.org/10.1093/mnras/stt2085)
- Tchekhovskoy, A., Narayan, R., & McKinney, J. C. 2011, *MNRAS*, 418, L79, doi: [10.1111/j.1745-3933.2011.01147.x](https://doi.org/10.1111/j.1745-3933.2011.01147.x)
- Trakhtenbrot, B., Arcavi, I., Ricci, C., et al. 2019, *Nature Astronomy*, 3, 242, doi: [10.1038/s41550-018-0661-3](https://doi.org/10.1038/s41550-018-0661-3)
- Wang, K., Liu, R.-Y., Li, Z., Wang, X.-Y., & Dai, Z.-G. 2022, *Universe*, 9, 1, doi: [10.3390/universe9010001](https://doi.org/10.3390/universe9010001)
- Werner, G. R., Uzdensky, D. A., Begelman, M. C., Cerutti, B., & Nalewajko, K. 2018, *MNRAS*, 473, 4840, doi: [10.1093/mnras/stx2530](https://doi.org/10.1093/mnras/stx2530)

- Xue, R., Liu, R.-Y., Petropoulou, M., et al. 2019, ApJ, 886, 23, doi: [10.3847/1538-4357/ab4b44](https://doi.org/10.3847/1538-4357/ab4b44)
- Xue, R., Liu, R.-Y., Wang, Z.-R., Ding, N., & Wang, X.-Y. 2021, ApJ, 906, 51, doi: [10.3847/1538-4357/abc886](https://doi.org/10.3847/1538-4357/abc886)
- Yuan, F., & Narayan, R. 2014, ARA&A, 52, 529, doi: [10.1146/annurev-astro-082812-141003](https://doi.org/10.1146/annurev-astro-082812-141003)
- Yuan, F., Quataert, E., & Narayan, R. 2003, ApJ, 598, 301, doi: [10.1086/378716](https://doi.org/10.1086/378716)
- Zathul, A. K., Moulai, M., Fang, K., & Halzen, F. 2024, An NGC 1068-Informed Understanding of Neutrino Emission of the Active Galactic Nucleus TXS 0506+056. <https://arxiv.org/abs/2411.14598>
- Zhang, B. T., Petropoulou, M., Murase, K., & Oikonomou, F. 2020, ApJ, 889, 118, doi: [10.3847/1538-4357/ab659a](https://doi.org/10.3847/1538-4357/ab659a)